E-ISSN 2586-9027
Homepage : https://tci-thaijo.org/index.php/SciTechAsia Science & Technology Asia
Vol.31 No.1 January - March 2026 Page: [211-243]
Original research article

Influence of Robot-assisted 3D-Printing Process Parameters on the Mechanical Properties, Structural Robustness, and Surface Finish of Clay and Sintered Clay

Nopporn Bukwan[1], Sasithorn Khonthon[2], Natt Makul[3,*]

[1]*Department of Manufacturing Technology, Faculty of Industrial Technology, Bangkok 10220, Thailand*
[2]*Department of Ceramic Technology, Faculty of Industrial Technology, Bangkok 10220, Thailand*
[3]*Department of Civil Engineering Technology, Faculty of Industrial Technology, Bangkok 10220, Thailand*

Received 23 December 2025; Received in revised form 16 February 2026
Accepted 23 February 2026; Available online 27 March 2026

ABSTRACT

This research investigates optimization of process parameters in robot-assisted three-dimensional (3D) printing of clay and sintered clay, focusing on nozzle diameter, print speed, layer height, and clay printability to improve mechanical strength, structural stability, and surface quality for sustainable architectural applications. Three nozzle sizes (3.0, 4.0, and 5.0 mm) were tested with print speeds from 100-500 mm/s and layer heights of LH60-160, while clay composites with controlled water-to-clay ratios were prepared to evaluate their effects on extrusion and structural performance. Results show that a smaller nozzle diameter of 3.0 mm combined with slower print speeds of 150-250 mm/s produced the strongest specimens, achieving compressive strengths up to 8.5 MPa and flexural strengths of 4.2 MPa while also generating smoother surfaces and more uniform layer deposition. Larger nozzles and higher speeds increased defects such as voids and cracks, reducing mechanical reliability. Lower layer heights (LH60) improved interlayer bonding and reduced porosity, whereas higher layers weakened adhesion. Optimal material performance occurred at 23.2% moisture content, balancing workability and structural stability. Excess moisture caused sagging while insufficient moisture increased extrusion resistance and cracking.

Keywords: Clay; Layer height; Mechanical properties; Nozzle diameter; Print speed; Robot-assisted 3D-printing

***Corresponding author:** natt@pnru.ac.th **doi:** xx.xxxxx/scitechasia.xxxx.xx

1. Introduction

The optimization of parameters related to clay-based 3D-printing, which utilizes robot-assisted extrusion techniques, necessitates the integration of cutting-edge technologies and sophisticated methodologies aimed at significantly enhancing the precision, overall efficiency, and adaptability of the entire printing process. This meticulous optimization is critically important for attaining outputs of exceptionally high quality and for broadening the scope of applicability of clay 3D-printing technologies [1], especially within vital industries such as construction and architecture, where innovative fabrication solutions are increasingly demanded [2, 3]. Through the careful refinement of these parameters, the manufacturing processes can effectively address and fulfill the rapidly growing demand for sustainable, customizable, and large-scale fabrication solutions that are becoming essential in today's environmentally-conscious market [4-7].

The integration of vision-based adaptive workflows in clay 3D-printing significantly enhances precision by utilizing computer vision and advanced algorithms to scan and reconstruct the robot's workspace in real-time. This approach accommodates complex surfaces and material behaviors, as demonstrated in the fabrication of interlocking components on re-configurable sand formworks [8]. Machine vision models analyze captured images and videos to detect defects, allowing automatic adjustments to improve print quality and reduce manual intervention [9]. Using reusable formworks, such as moldable sand, further promotes sustainability by offering a customizable, eco-friendly fabrication solution [10-13]. Parametric design integration enhances flexibility through tailored algorithms for adaptable toolpath planning, optimizing robotic movements while maintaining design expression [14, 15]. In combination with industrial extruders, this workflow ensures precise clay deposition, supported by real-time feedback systems to adjust print parameters and enhance accuracy [16]. Despite challenges in computer vision systems due to factors like lighting and occlusions, advanced simulations and predictive models help optimize fabrication, demonstrating the potential of this technology for sustainable architectural design [17].

Multi-axis clay 3D-printing represents a significant advancement in fabricating complex ceramic structures, providing enhanced design flexibility and precision. This technology utilizes customized extruders and multiple end-effectors to accommodate varying material viscosities, optimizing key parameters like extrusion velocity, nozzle diameter, and printing speed [18, 19]. These adjustments reduce extrusion resistance and ensure uniform layer deposition, improving surface quality and structural integrity [20-24]. Advanced algorithms, such as BP neural networks and hybrid neural networks, are employed to fine-tune these parameters, further reducing surface roughness and enhancing dimensional accuracy [25, 26]. Additionally, sustainable techniques like robotic milling and liquid clay deposition enhance environmental and cost efficiency, positioning clay-based 3D-printing as a viable solution for eco-friendly construction [27, 28].

The integration of multi-axis systems, like five-axis FDM, addresses challenges such as the staircase effect and material overuse, improving surface quality and reducing material consumption [18]. Coextrusion techniques also allow for gradient porosity in ceramic structures, improving insulation and acoustics in archi-

tectural applications [29]. However, challenges like achieving defect-free, dense ceramic components and the need for post-processing continue to hinder widespread adoption [30-34]. Despite these obstacles, the use of advanced optimization algorithms and sustainable fabrication techniques suggests that multi-axis clay 3D-printing holds significant promise for producing complex, eco-friendly structures in architecture and construction. While the optimization of clay-based 3D-printing parameters through robot-assisted extrusion offers numerous advantages, challenges remain in terms of scalability and integration into existing construction practices [35]. The complexity of multi-axis printing and the need for precise control over material properties require continued research and development. Additionally, the adoption of these advanced techniques within the industry may be hindered by high initial costs and the requirement for specialized equipment and expertise [36-38]. However, the potential for sustainable, customizable construction solutions makes this an exciting area for future innovation and exploration [39, 40]. This research examines the enhancement of process parameters in robot-assisted three-dimensional (3D) printing of clay and sintered clay, focusing on nozzle diameters, print speed, layer heights, and clay printability. The objective is to improve the mechanical characteristics, structural stability, and surface finish of produced clay artifacts for utilization in sustainable architecture. Three nozzle diameters were evaluated in conjunction with differing print speed and layer heights. Clay composites with a water-to-clay ratio were formulated to assess their effect on printability and performance.

2. Materials and Methods

2.1 Materials

The primary material used in this study is a clay-based mixture (Fig. 1). Clay preparation was performed by conditioning Terracotta clay (Extrusion Clay Body, ECB) received from Singburi province of Thailand, with a moisture content of about 23.2% (wet basis). The clay mixture was sealed in an airtight container and allowed to rest for 24 hours. After conditioning, the material was hand-kneaded for a minute to achieve a homogenous appearance. Then, the printability of the clay was assessed by filament extrusion for shape retention and deposition stability. Moisture content was assessed using a wet method in accordance with ASTM C324 [41]. The oxide composition of clay profoundly influences its properties, making it suitable for diverse applications like ceramics, construction, and 3D-printing. Silicon dioxide (SiO_2) constitutes 64.40% of the clay, acting as the primary structural component that enhances the material's hardness, durability, and resistance to high temperatures, as shown in Table 1. This high silica content provides stability to clay-based structures, especially valuable in applications involving sintering, as it contributes to forming a rigid matrix upon drying and firing. Aluminum oxide (Al_2O_3), present at 23.40%, adds to the clay's mechanical strength and thermal resistance. Its plasticity, when mixed with water, aids in shaping and molding, a critical attribute in forming processes and applications requiring flexibility, such as 3D-printing. Al_2O_3 also strengthens the clay's resistance to chemical degradation, making it ideal for use in chemically harsh environments. Iron oxide (Fe_2O_3) at 5.50% imparts a reddish color upon firing and increases the density and toughness for applications needing precise geometry.

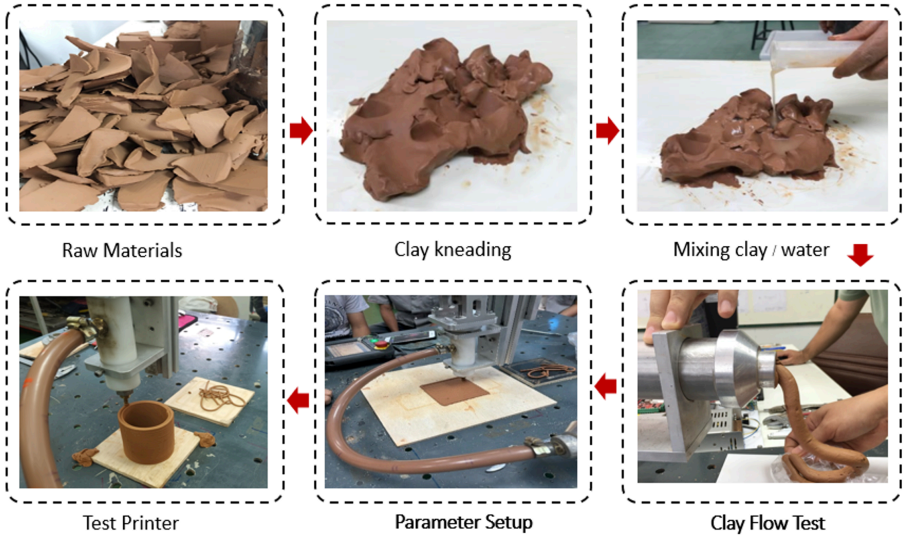

Fig. 1. Natural clay used as the raw material for robot-assisted 3D-printing experiments.

Potassium oxide (K_2O) at 2.70% serves as a fluxing agent, diminishing the clay's melting temperature and facilitating energy-efficient sintering by promoting vitrification, which culminates in a dense, glassy and impermeable surface optimal for non-porous ceramic applications. Titanium dioxide (TiO_2) at 0.81% augments opacity, yielding a whiter, UV-resistant finish appropriate for aesthetic considerations in ceramics and constructions exposed to solar radiation. Magnesium oxide (MgO) at 0.80% enhances thermal stability, functioning as a refractory to regulate shrinkage during firing, thereby preserving dimensional integrity. Sodium oxide (Na_2O) at 0.72% operates analogously to K_2O, assisting in sintering and augmenting structural density and environmental resilience. Calcium oxide (CaO) at 0.71% contributes to fluxing and fortifies the matrix, diminishing the risk of cracking during drying and firing, which is critical for structural reliability. Phosphorus pentoxide (P_2O_5) at 0.66% enhances binding uniformity, while Manganese oxide (MnO) at 0.07% affects coloration without significantly altering structure. Rubidium oxide (Rb_2O), at trace concentrations (0.04%), exerts minimal influence on thermal and structural properties. This oxide configuration equilibrates strength, durability, and aesthetics, augmenting stability and precision. The elevated SiO_2 and Al_2O_3 content ensures robust structural integrity, rendering the clay suitable for energy-efficient sintering, 3D-printing, and advanced industrial and architectural applications necessitating consistent performance under diverse conditions.

2.2 Robotic extruder setup: Design and optimization of clay printing system

This design and construction of a clay 3D-printing system utilizes a 6-axis robotic arm. The printing system design is partitioned into two components: extruder and controller (Fig. 3(a)). A clay extruder serves as a framework and mechanism for extruding and combining clay so that it can emanate from the injection aperture consistently and homogeneously. The

Table 1. Chemical composition of clay.

Oxide	SiO_2	Al_2O_3	Fe_2O_3	K_2O	TiO_2	MgO	Na_2O	CaO	P_2O_5	MnO	Rb_2O
Mass%	64.40	23.40	5.50	2.70	0.81	0.80	0.72	0.71	0.66	0.07	0.04

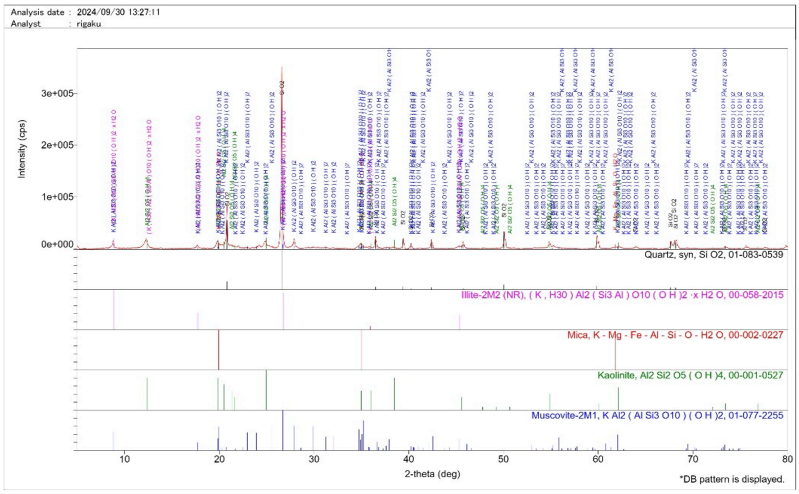

Fig. 2. XRD patterns of natural clay.

extrusion system comprises the extrusion and the mixing systems. The clay extrusion system's operational principle commences with the clay's introduction into the clay cylinder with the suitable clay/water amalgamation ratio. Subsequently, the clay extrusion system depends on the operation of the screw to extrude the clay within the cylinder. The screw possesses a diameter of 14.0 mm. The screw is affixed to a gear block with a gear ratio of 10:1. To regulate the flow of clay during this process, an automated control system is employed. Utilizing a control program to govern the control system enables it to function continuously. The apparatus employed to manage the system comprises: 1. Stepper motor, model Nema 23, connected to a gear block assembly and possessing an internal thread that modifies the direction of angular movement (Angle Rotation) to linear displacement (Linear motion) so that the system can extrude the clay appropriately. The motion control of the clay extrusion system utilizes a control program (Mach3 CNC Controller) through a computational device. By overseeing the operation of the clay extrusion system, when the control system receives a command/code, the code or program will utilize the format G01 A1000000 F500. Once the program is inscribed, the control program will transmit a signal to the microcontroller board (RnR Motion Control) connected via a USB interface to command the micro-step driver, model DM542, to activate the motor connected to the screw assembly. Upon receiving a signal to activate the motor, the extrusion system will extrude through the screw, resulting in the clay flowing from the injection aperture.

The injection aperture at the terminus of the soil filling cylinder has a diameter of 16.0 mm. The amalgamation of the soil extrusion apparatus with the soil mixing apparatus at this juncture will employ a water conduit. It has a length of 800.0 mm,

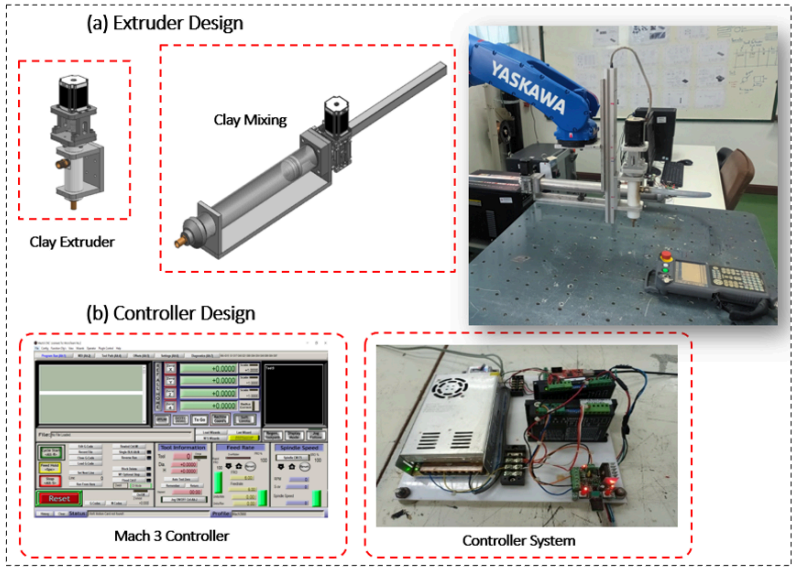

(a) Design Extruder for 6-axis robot arm clay printing

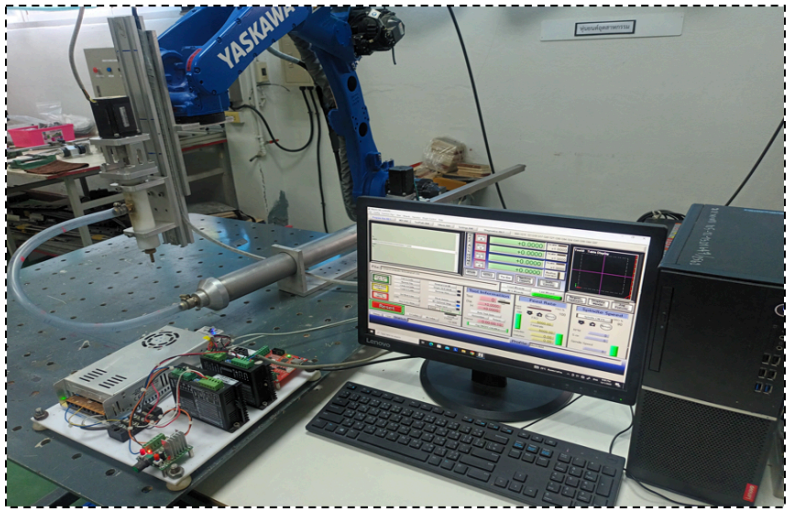

(b) Robotic extruder setup

Fig. 3. Robotic clay extrusion system for a 6-axis robot arm: (a) detailed design of the extrusion mechanism and (b) assembled robotic extruder and printing setup used in the experiments.

an external diameter of 20.0 mm, and an internal aperture of 16.0 mm. It is affixed to the soil mixing cylinder, which has an engineered external diameter of 30.0 mm, a length of 200.0 mm, and an internal aperture of 16.0 mm. The operational principle of the soil mixing apparatus is that when the clay traverses through the conduit into the soil mixing cylinder assembly, it facilitates the disintegration of the soil. A screw assembly is employed for the mixing process, wherein the screw thread utilized has

a diameter of 14.0 mm and a pitch of 10.0 mm. The regulation of the mixing process for the screw thread assembly employs a motor speed modulation device (Speed Control) linked to a Nema 23 stepper motor and a micro-stepping driver (Micro-step Driver), model DM542. As the extrusion assembly propels the clay through the soil mixing assembly, the mixing assembly will blend the soil to facilitate its disintegration and allow it to escape from the nozzle assembly (Nozzle). At the terminus of the soil filling apparatus, the nozzle can be altered to accommodate the desired dimensions. In the design of this extruder assembly, a computer-aided design (CAD) program will be utilized to configure the extrusion assembly components. Subsequently, the principal and ancillary components will be integrated into the computer (Assembly). The requisite equipment will be procured upon attaining a comprehensive extrusion assembly model, and a clay printing system for the 6-axis robotic arm will be developed. Once the equipment assembly is constructed in accordance with the model, the extrusion unit will be installed on the Yaskawa AR1440 6-axis robotic arm (Fig 3(b)).

The Yaskawa AR1440 [42] is a high-speed, six-axis welding robot optimized for productivity and precision in industrial applications. With a payload capacity of 12.0 kg, a horizontal reach of 1,440.0 mm, and a vertical reach of 2,511.0 mm [43,44], it provides ample flexibility for complex welding tasks. Its streamlined arm design minimizes interference, while an expanded wrist range enhances accessibility in tight spaces, making it suitable for high-density work cells. The AR1440 achieves a repeatability of 0.02 mm, ensuring high accuracy, and features a 50.0 mm thru-hole for effective cable management, reducing wear and extending cable life. Powered by the YRC1000 controller [45], the robot supports intuitive programming and the control of up to eight robots and multiple positioners, facilitating synchronized motion across systems. Advanced programming functions enhance weld quality and speed, while optional add-ons like vision systems and seam tracking offer customization. This combination of robust specifications, innovative design, and flexible control capabilities makes the AR1440 ideal for efficient, high-quality automated welding operations [46].

The architecture of the extruder in multi-axis clay additive manufacturing is paramount for guaranteeing precise material deposition, accommodating diverse material viscosities, and attaining the requisite structural integrity of the fabricated objects. An optimally engineered extruder generally comprises several fundamental components: the nozzle, the feeding mechanism, and the thermal system, all of which function synergistically to regulate the flow and uniformity of the clay throughout the additive manufacturing process.

- Nozzle: The dimensions and configuration of the nozzle directly influence the extrusion of the clay. In multi-axis additive manufacturing, nozzle dimensions are meticulously chosen to enhance material flow and ensure consistent layer deposition. Nozzle diameters may vary from 3.0 mm to 5.0 mm, whereby smaller nozzles provide superior layer resolution and augmented precision, while larger nozzles facilitate accelerated printing but may jeopardize detail. The nozzle's design is also tailored to mitigate clogging, improve flow regulation, and assure consistent extrusion under fluctuating pressures.

- Feed Mechanism: The extruder is outfitted with a robust feeding system, frequently employing either a screw-driven or piston-driven mechanism, to propel the clay through the nozzle. This mechanism must possess the capacity to accommodate varying material viscosities and ensure a smooth, uninterrupted flow. In high-precision configurations, the print speed can be dynamically modulated to optimize printing speed and resolution.

- Material handling and viscosity control: For clay-based additive manufacturing, the extruder must be engineered to manage the specific rheological characteristics of clay. This encompasses regulating the moisture content, additives, and overall consistency of the material. The extruder design may incorporate sensors or feedback systems to monitor viscosity and adjust extrusion pressure in real-time to compensate for any fluctuations in the material during the printing operation.

- Adaptability and multi-end effectors: In sophisticated extruder designs, multiple end-effectors can be integrated to transition between diverse materials or nozzle dimensions during a singular print task. This capability facilitates enhanced flexibility in material application and is particularly advantageous in architectural contexts where varying structural and aesthetic requisites may necessitate the utilization of distinct clay formulations or layer thicknesses.

The extruder was mounted on a robotic arm, allowing precise control over the material deposition process. The system's configuration and the printing process were optimized by adjusting the nozzle diameter, print speed and layer height. The extruder was equipped with interchangeable nozzles to evaluate how nozzle diameter affects the final product's mechanical properties and printing efficiency.

- Nozzle diameters: 3.0, 4.0, and 5.0 mm

- Print speed: Varying from 100 to 500 mm/s with a constant extrusion velocity of 500 mm/s.

- Layer Height: Parameters for the layer height were set between LH60 and LH160 depending on the nozzle diameter.

As shown Fig. 4, the optimization of the 3D-printing process was conducted through systematic variations of key parameters:

- Extrusion Velocity: Adjusted between 150 to 500 mm/s.

- Layer Height and Step Over: Each nozzle diameter was tested with different layer heights (LH60 to LH160) and step-over values between 80% and 160% of the nozzle diameter.

- Print speed parameters: The nozzle print speed was adjusted based on nozzle diameter to ensure uniform material deposition and minimize extrusion resistance.

The preparation of the CAD/CAM (Computer-Aided Design/Computer-Aided Manufacturing) program is a crucial step in multi-axis clay 3D-printing, as it involves the conversion of design models into executable commands for the robotic printer.

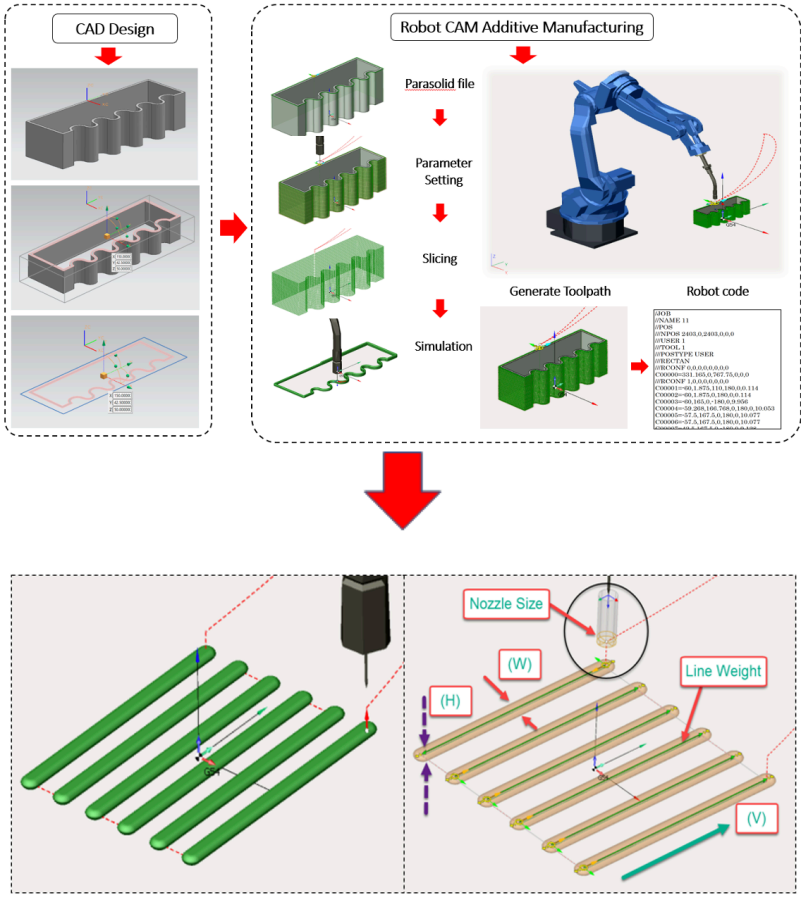

Fig. 4. Parametric adjustments.

This process ensures that the design intent is accurately translated into physical structures, optimizing toolpath planning, material deposition, and overall print quality. The CAD/CAM workflow integrates both design flexibility and manufacturing precision, allowing for the complex geometries typical in clay 3D-printing projects [26, 47].

(i) Designing in CAD: The first step involves creating a digital model using CAD software This model serves as the blueprint for the final printed object, encompassing its geometric dimensions, surface details, and structural features. In architectural applications or custom ceramics, these designs often feature intricate curves, overhangs, or complex patterns that require careful planning to print accurately. Designers can also use parametric design tools in the CAD environment to automate adjustments based on input variables, enabling the creation of multiple design iterations with varying dimensions or structural properties.

(ii) Toolpath Planning in CAM: Once the CAD model is finalized, the CAM software takes over, converting the design into a series of toolpaths that

the robot or printer will follow. This step includes determining the optimal nozzle paths, layer heights, and material deposition rates based on the object's geometry and material properties. CAM software allows users to define key parameters such as extrusion speed, nozzle diameter, and layer orientation, which are vital for achieving high-quality prints with minimal defects. For multi-axis printing, this planning becomes more complex, as the system must account for various angles and orientations to minimize support structures and improve surface finish.

(iii) Simulation and Validation: Before sending the toolpath to the printer, simulations are run to visualize the printing process in a virtual environment. This allows for the detection of potential issues such as collisions, over-extrusion, or layer misalignment. The simulation ensures that the path is optimized for efficiency and precision, reducing the likelihood of errors during the actual printing. Additionally, CAM software can simulate material behavior to predict how the clay will behave under different environmental conditions (e.g., drying, shrinkage), helping to process.

(iv) Generating Robot-code: After validating the toolpath, the CAM program converts the instructions into Robot-code, the language used by 3D-printers and CNC machines. This code includes all the necessary commands for the robotic printer, such as movement coordinates, extrusion rates, and speed adjustments, ensuring precise control over the entire printing process.

(v) Integration with Robotic Control: In multi-axis clay 3D-printing, the CAD/CAM program must also be compatible with the robotic arm's control system. This involves synchronizing the robotic movements with the toolpath generated by the CAM software, ensuring smooth transitions between different printing angles and complex geometries. The program also needs to manage real-time adjustments to compensate for any unexpected material behavior or environmental factors, such as clay viscosity changes or temperature variations.

2.3 Design of experiments (DOE)

The independent variables were described by the experimental design from two level factorial design (2^k), with three major factors: nozzle diameter, print speed, and layer height, summarized in Table 2. Nozzle diameters of 3.0, 4.0 and 5.0 mm; print speed 250, 350 and 450 mm/min; layer height ratios 60, 100 or 120% as a function of nozzle diameter with each factor tested in three levels. Using a six-axis robotic arm, a specimen was printed for each experimental condition and parameter combination listed in Table 2. Apart from the investigated factors, the controlled variables remained constant: the screw turning speed within the nozzle (extrusion velocity, fixed at 500 mm/s) and the water-to-clay ratio, set to a moisture content of 23.2% (wet-basis). It was to compare and determine relationships among the printing parameters on the one hand, and the response variables (printing quality and structural integrity) as controls on the other. Every examination was

performed twice. The printed specimen geometry was a square prism with dimensions (width × length × height) of 100 mm × 100 mm × 100 mm.

Table 2. Experimental factors and levels.

Factors	Level		
	Low	Medium	High
Nozzle Diameter (mm)	3	4	5
Print speed (mm/s)	250	350	450
Layer height (%)	60	100	120

2.4 Parametric adjustments

The 3D-printed specimens were subjected to thermal treatment at 1150 °C within an oxidizing atmosphere utilizing a Nabertherm electric furnace, as shown in Fig. 5, which functions within a thermal spectrum of 30-1300 °C, ensuring meticulous regulation over the heating profile. The thermal firing procedure was conducted with a regulated heating rate of 3.0 °C per minute, progressively elevating the temperature to avert thermal shock and to guarantee homogeneous heat distribution throughout the specimens. Furthermore, the extensively utilized chamber kilns are purposefully engineered for rigorous industrial functions like annealing, hardening, and forging, with tri-faceted radiation heating that guarantees thermal uniformity (± 10 °C). They exhibit robust construction, SiC-guarded basal heating, multilayer insulation for energy optimization, and a stainless-steel portal for thermal resistance. They ensure safety and precision by furnishing gas-damped portals, a thermal limiter, and a B500 touch controller with data archiving. The kilns adhere to safety standards, excluding perilous refractory ceramic fibers, and may be tailored for particular applications.

The gradual heating methodology also facilitated appropriate densification and phase transformation phenomena, which are imperative for attaining the requisite microstructural and mechanical characteristics. The aggregate duration of the firing cycle, encompassing the heating, soaking, and cooling phases, was approximately 6.0 hours. The retention period at the peak temperature of 1150 °C permitted adequate time for the comprehensive oxidation reactions and stabilization of the material's crystalline phases.

2.5 Testing methods

After sintering, specimens were subjected to mechanical testing to evaluate their structural properties. These tests allowed for a thorough analysis of the printed structures, helping to establish the relationship between material composition, extruder settings, and mechanical performance.

- Flexural strength test: A three-point flexural test was performed to evaluate the mechanical resistance of the 3D-printed structures in compliance with ASTM C1161 [48]. Rectangular bar specimens with dimensions of 25 mm × 100 mm × 25 mm (Configuration B) were used and tested at a constant crosshead speed of 0.5 mm/min. The test was conducted using a support span of 60 mm, as shown in Fig. 6(a)

- Compressive strength test: Specimens were tested under axial compressive load to determine the maximum load-bearing capacity prior to structural failure, in accordance with ASTM C1424 [49]. Cubic specimens measuring 50 mm × 50 mm × 50 mm were used and subjected to a constant loading rate of 0.5 mm/min. The testing configuration was designed

Fig. 5. 3D-printed clay specimens subjected to the sintering process.

to ensure uniform stress distribution across the printed layers, as shown in Fig. 6(b).

- Water Absorption Test: Each specimen was tested for water absorption to evaluate its porosity and potential for water retention in compliance with ASTM C373 [50].

The mechanical test results were analyzed using statistical methods to identify correlations between nozzle diameter, print speed, and the resulting mechanical properties. This data-driven approach ensured that optimal printing parameters could be identified to achieve high-quality, structurally sound clay-based 3D-printed specimens.

3. Results and Analysis

3.1 Influences of nozzle diameters, print speed, layer heights on clay printability

3.1.1 Relationship between nozzle diameter and print speed (W/H)

Fig. 7 shows the printed patterns between nozzle/print speed (W/H) The relationship between nozzle diameter and print speed (W/H) is fundamental in optimizing the quality and precision of clay 3D-printing. Nozzle diameter dictates the width of the material being extruded, while the print speed controls how quickly this material is deposited. Smaller nozzles, such as 3.0 mm, require slower print speed (150-250 mm/s) to maintain fine resolution and prevent under-extrusion, which ensures better surface finish and stronger interlayer bonding. Larger nozzles, like 4.0 or 5.0 mm, allow for faster material deposition but require higher print speed to avoid over-extrusion and maintain consistency. Balancing these parameters is essential for producing defect-free prints, as mismatches can result in poor layer adhesion, uneven heights, or surface defects. This balance must also account for material properties like viscosity to ensure uniform deposition and strong, durable structures [51, 52].

The parameter correlation between nozzle dimensions and print speed (W/H) in clay three-dimensional printing is paramount for regulating the flow and deposition of substances. This correlation directly impacts the caliber, resolution, and structural coherence of the fabricated object. The nozzle dimensions dictate the breadth (W) of the extruded substance, while the print speed, frequently articulated in terms of speed (H), governs the pace at which the material is deposited. Adequate synchronization between these two parameters guarantee uniform layer deposition, minimizes extrusion resistance, and augments interlayer adhesion, all of which

Fig. 6. (a) Flexural strength test and (b) Compressive strength test.

contribute to the mechanical robustness and precision of the printed configuration.

For miniscule nozzles (e.g., 3.0 mm), reduced print speed (approximately 150-250 mm/s) is conventionally favored to sustain fine resolution and consistent material flow. This culminates in enhanced surface finish and more precise layer stacking, particularly in intricate or elaborate designs. In contrast, larger nozzles (e.g., 4.0 or 5.0 mm) necessitate elevated print speed to prevent over-extrusion and ensure that material is deposited at an adequate rate to correspond with the augmented material flow. Nonetheless, excessive print speed can induce defects such as inadequate bonding between layers or non-uniform layer height, thereby compromising print quality. The equilibrium between nozzle dimensions and robotic feed velocity must be meticulously calibrated depending on the material characteristics, such as viscosity and workability, to optimize the printing process for diverse clay mixtures and design specifications [53].

3.1.2 Layer height (LH)

The layer height in clay 3D-printing plays a crucial role in determining the surface quality, structural integrity, and overall efficiency of the printing process. As shown in Fig. 8, the smaller layer heights (e.g., 60-100 microns (μ)) result in finer resolution, creating smoother surfaces with more accurate detail reproduction [54]. This increased precision improves interlayer bonding, as each layer is closer together, allowing for better adhesion and reduced chances of defects such as voids or gaps. Stronger interlayer adhesion enhances the mechanical properties of the printed object, particularly in terms of compressive and flexural strength. However, using smaller layer heights also increases printing time, as more layers are required to build the object, making it less efficient for larger-scale projects [55,56]. On the other hand, larger layer heights (e.g., 150-200 microns (μ)) reduce the overall print time by depositing more material with each pass, making the process faster and more suitable for bulkier objects or when fine detail is less critical. However, larger layers can lead to poorer surface quality, with more pronounced layer lines and potential issues in bonding between layers. This weakens the interlayer cohesion and can result in reduced mechanical performance, particularly in terms of strength and durability. Additionally, larger layer heights increase the likelihood of geometric inaccuracies, as the thicker layers may sag or deform under their own weight, especially with more fluid

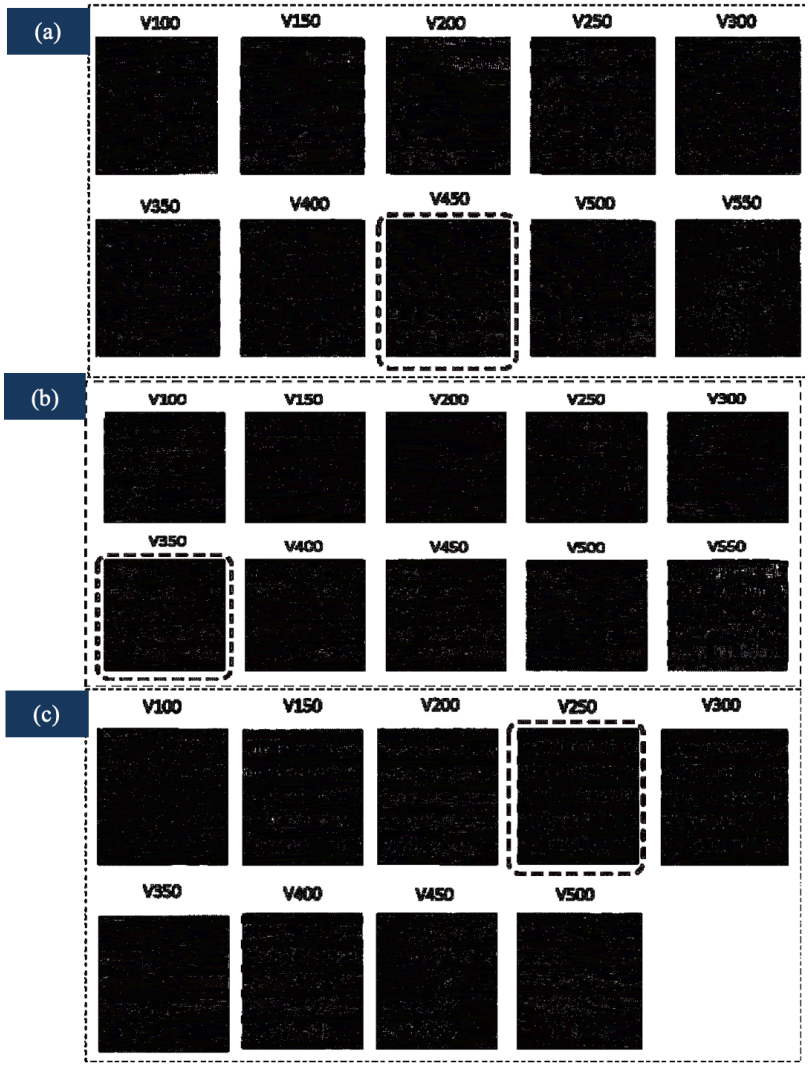

Fig. 7. 3D-printing specimen patterns between nozzle/ print speed (W/H): (a) Nozzle diameter of 3.0 mm, V = 100-500 mm/s, (b) Nozzle diameter of 4.0 mm, V = 100-500 mm/s, and (c) Nozzle diameter of 5.0 mm, V = 150-500 mm/s.

or viscous clay mixtures [57,58]. Thus, while larger layer heights improve printing speed, they often compromise the precision and structural integrity of the printed object, making the choice of layer height a critical factor that must be carefully balanced depending on the design requirements and material properties.

3.1.3 STEP over

As shown in Fig. 9, the STEP over, a pivotal parameter in clay three-dimensional printing, pertains to the percentage overlap between contiguous passes of the nozzle, and it directly influences surface finish, print quality, and material efficiency. A reduced STEP Over (typically 10-50%) results in augmented overlap between passes, yielding a more refined surface finish and

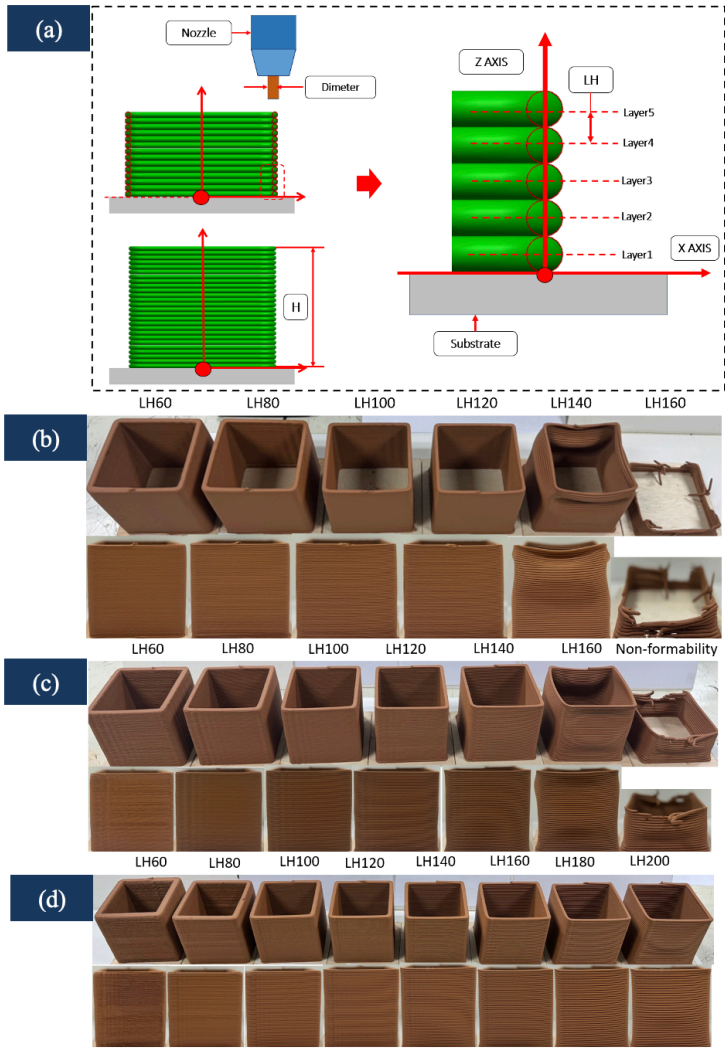

Fig. 8. Layer height printing patterns under different nozzle configurations: (a) Layer height (LH), (b) Nozzle diameter of 3.0 mm, V= 100-500 mm/s, LH60-LH160, (c) Nozzle diameter of 4.0 mm, V= 100-500 mm/s, LH60-LH160, and (d) Nozzle diameter of 5.0 mm, V= 100-500 mm/s, LH60-LH200.

enhanced uniformity in layer deposition. This elevated overlap guarantees that any interstices between passes are minimized, diminishing the probability of voids and discontinuities in the final print. The increased overlap also fosters interlayer adhesion, particularly when addressing intricate geometries or elaborate designs that necessitate precise material deposition. Nevertheless, a diminished STEP Over value also decelerates the printing process, as the nozzle must undertake additional passes to cover the same area, thereby extending production time and potentially escalating material costs [59]. On the other hand, an expanded STEP Over (exceeding 50%) permits the nozzle to encompass a greater area with each pass, markedly accelerating the printing process and rendering it more efficient for large-scale projects. How-

ever, this heightened velocity is accompanied by trade-offs in print quality. An increased STEP Over can result in conspicuous gaps between passes, culminating in a rougher surface finish and diminished cohesive layer formation. These interstices not only compromise aesthetics but also engender potential vulnerabilities in the printed structure, particularly concerning mechanical properties such as tensile and compressive strength [60]. In extreme scenarios, inadequate overlap can precipitate delamination or even structural failure under load. For this rationale, larger STEP over values are frequently only appropriate for objects where surface quality and fine details are of lesser significance, or where speed is prioritized over precision.

The selection of STEP Over also interacts with other process parameters, such as nozzle dimension, print speed, and layer height, rendering it essential to equilibrate these factors in accordance with the specific project requirements. For instance, employing a larger nozzle or thicker layer height in conjunction with a high STEP Over can exacerbate surface defects and compromise the structure, while a smaller nozzle or thinner layer height combined with a reduced STEP Over enhances surface quality but retards the process [61]. Material characteristics, such as the viscosity of the clay, also exert influence: more fluid mixtures may adequately fill gaps with a larger STEP Over, whereas thicker materials may not flow as readily, augmenting the risk of suboptimal layer adhesion. Therefore, optimizing the STEP Over is a critical determinant in achieving the desired equilibrium between speed, surface quality, and structural integrity in clay three-dimensional printing.

3.1.4 Statistical analysis of variance (ANOVA) for the width and height of 3D-printed clay specimens using a robotic system

A statistical analysis of variance (ANOVA) was conducted to evaluate the effects of the investigated printing parameters on the dimensional accuracy and overall quality of the 3D-printed clay specimens-the analysis aimed to determine which factors significantly influenced the measured responses, specifically specimen width and height. A confidence level of 95% (α = 0.05) was adopted to assess statistical significance.

The ANOVA results were further applied to the regression model for specimen width (W) (Table 3) and height (H) (Table 4) to examine the suitability and predictive capability of the developed model. The statistical significance of the model terms, including main effects and potential interactions, was evaluated based on the F-value and corresponding p-value. Factors with p-values less than 0.05 were considered statistically significant contributors to dimensional variation.

3.2 Physical and mechanical properties

The second phase of the comprehensive study undertook an extensive investigation into the intricate relationships among nozzle diameter, print speed, and layer height, specifically focusing on how these parameters collectively influenced the mechanical properties inherent to the printed clay structures. In this rigorous analysis, nozzle diameters measuring 3.0, 4.0, and 5.0 mm were systematically tested, while the print speeds were varied within a range extending from 100 mm/s to 500 mm/s, thereby providing a broad spectrum for examination.

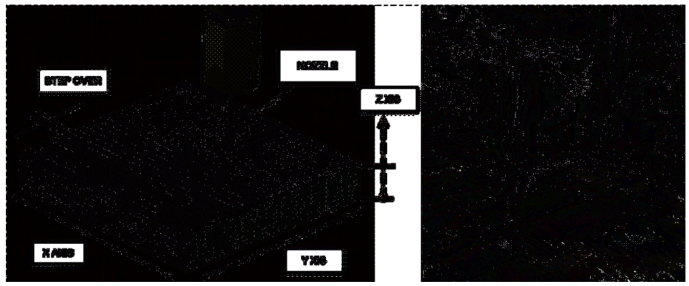

(a) STEP over

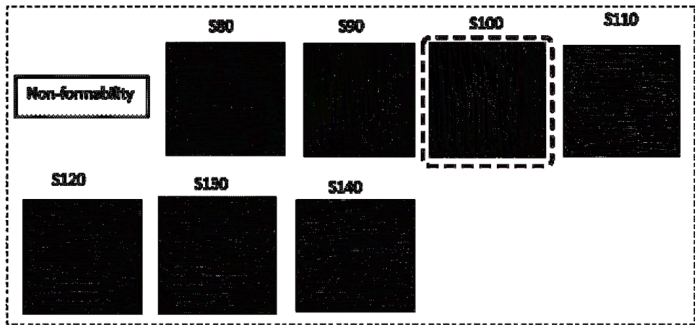

(b) Printed specimens

Fig. 9. Process parameters used in robot-assisted 3D-printing: Nozzle diameters of 3.0, 4.0, and 5.0 mm; print speed ranging from 100 to 500 mm/s; and step-over ranging from as 80-140% of the nozzle diameter.

Table 3. Statistical analysis of variance (ANOVA) of the regression model (W).

Source	DF	Adj SS	Adj MS	F-Value	*P*-Value
Model	26	32.7685	1.2603	330.7	0
Linear	6	31.4897	5.2483	1377.1	0
Nozzle	2	5.143	2.5715	674.74	0
Print Speed	2	23.5085	11.7542	3084.2	0
Layer Height	2	2.8382	1.4191	372.36	0
2-Way Interactions	12	0.528	0.044	11.54	0
Nozzle∗Print Speed	4	0.2938	0.0735	19.28	0
Nozzle∗Layer Height	4	0.13	0.0325	8.53	0
Print Speed∗Layer Height	4	0.1041	0.026	6.83	0.001
3-Way Interactions	8	0.7508	0.0939	24.63	0
Nozzle∗Print Speed∗Layer Height	8	0.7508	0.0939	24.63	0
Error	27	0.1029	0.0038		
Total	53	32.8714			
R^2			99.69%		
Mean			4.09		
StDev			0.79		

Remark: *p*-value less than 0.05 indicates statistical significance.

3.2.1 Water absorption

were meticulously conducted to assess the printed structures' porosity characteristics. The findings derived from these tests unequivocally indicated that implementing larger nozzle diameters in conjunction with higher layer heights significantly contributed to increased printed specimens' porosity, consequently resulting in elevated water absorption rates [6, 62, 63]. At a 3.0 mm nozzle diameter, water absorption equals 18.0%, reflecting relatively moderate porosity levels. At a 4.0 mm nozzle diameter, water absorption is 22.0%, indicating a noticeable increase in porosity compared to the 3.0 mm nozzle diameter. At a 5.0 mm nozzle diameter, water absorption is 25.0%, representing the highest level of water absorption among the tested nozzle diameters. In a manner analogous to the influence of nozzle diameter, the employment of higher layer heights resulted in an augmented water absorption capacity, with LH160 specimens absorbing as much as 28.0% of their weight in water, a stark contrast to LH60 specimens, which demonstrated a lower absorption rate of only 16.0%.

3.2.2 Compressive strength

As shown in Fig. 10, the utilization of the 3.0 mm nozzle diameter resulted in the production of structures exhibiting the highest compressive strength, a phenomenon attributed to the finer layer deposition, which subsequently facilitated a higher density within the printed constructs. Conversely, applying the 5.0 mm nozzle diameter yielded structures of comparatively weaker integrity, as the more extensive layers demonstrated a notable deficiency in cohesion amongst themselves, ultimately compromising structural integrity. For a 3.0 mm nozzle, the maximum compressive strength is 8.5 MPa, which represents the pinnacle of strength attainment in this experimental framework. At a 4.0 mm nozzle diameter, the maximum compressive strength is 6.8 MPa, indicating a significant decrement when juxtaposed with the 3.0 mm nozzle diameter results. While for a 5.0 mm nozzle diameter, the maximum compressive strength is 5.2 MPa, reflecting the least robust performance among the tested nozzles.

The imposition of slower print speeds, particularly those within the range of 100 to 250 mm/s, yielded structures of enhanced strength, a result attributable to the extended temporal allowance afforded for optimal material deposition and enhanced bonding between layers. In stark contrast, elevated print speed precipitated a marked decline in compressive strength, with the resultant layers exhibiting insufficient adhesion, thereby undermining structural integrity. Print speeds of 150-250 mm/s, represented the most favorable conditions for achieving superior mechanical properties [64-66].

3.2.3 Flexural strength

As shown in Fig. 10, the flexural strength exhibited a trend remarkably analogous to that of compressive strength, with smaller nozzle diameters conferring a superior ability to resist flexural loads, an outcome stemming from the production of smaller layers that resulted in more compact and cohesive structures. For a 3.0 mm nozzle diameter, the flexural strength of 4.2 MPa is indicative of the exemplary performance observed within this category. For a 4.0 mm nozzle diameter, the flexural strength is 3.4 MPa, which, while lower, still demonstrates considerable resistance compared to larger sizes. For a 5.0 mm nozzle diameter, the flexu-

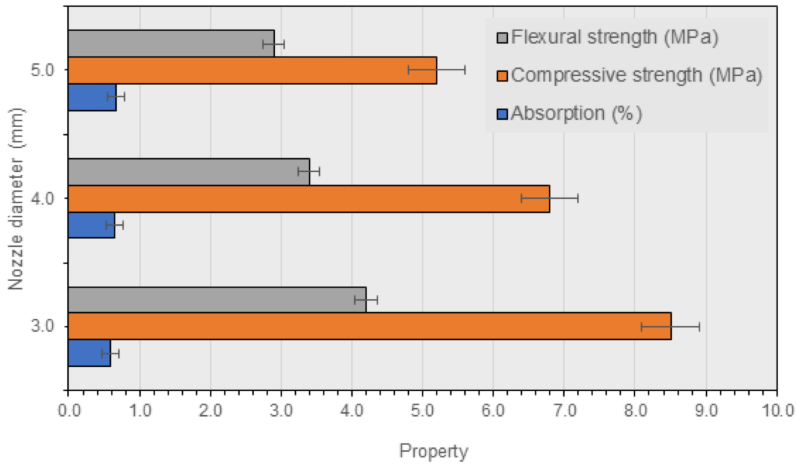

Fig. 10. Flexural strength, compressive strength, and water absorption of clay specimens 3D-printed using different nozzle diameters.

ral strength of 2.9 MPa shows the least resilience to flexural forces among the tested nozzles. The printed structures utilizing smaller layer heights, identified explicitly as LH60, exhibited a marked increase in flexural strength attributable to the more compact stacking of layers and a reduction in void formation. In contrast, applying more considerable layer heights, such as LH160, led to an observable weakening of bonding between layers, culminating in reduced flexural strength.

3.3 Visual analysis of printed clay specimens

The visual analysis of 3D-printed clay specimens provides critical insights into the relationship between printing parameters and the resulting structural quality of the objects. This analysis focuses on surface finish, layer consistency, and the presence of defects such as voids, cracks, and sagging, which can significantly influence the mechanical properties and overall integrity of the printed structures. Through a comprehensive examination of the specimens produced under varying process conditions—such as nozzle diameter, print speed, and layer height—distinct patterns emerge regarding how these parameters affect the visual and structural characteristics of the printed clay objects. This section outlines the key observations from the visual analysis, correlating them with the mechanical performance and providing a foundation for understanding the optimization of clay 3D-printing in a robotic extrusion context as shown in Fig. 11.

One of the most immediately apparent outcomes of the visual analysis is the effect of nozzle diameter on the surface finish and consistency of the printed layers. Specimens produced using smaller nozzles (3.0 mm) exhibited smoother, more uniform surfaces, with well-defined layer boundaries and minimal visible defects as shown in Fig. 11(a). This improved surface quality can be attributed to the finer extrusion resolution provided by the smaller nozzle, which allows for more precise material deposition. As the nozzle diameter increased (4.0 mm (Fig. 11(b)) and 5.0 mm (Fig. 11(c)), the surface finish became progres-

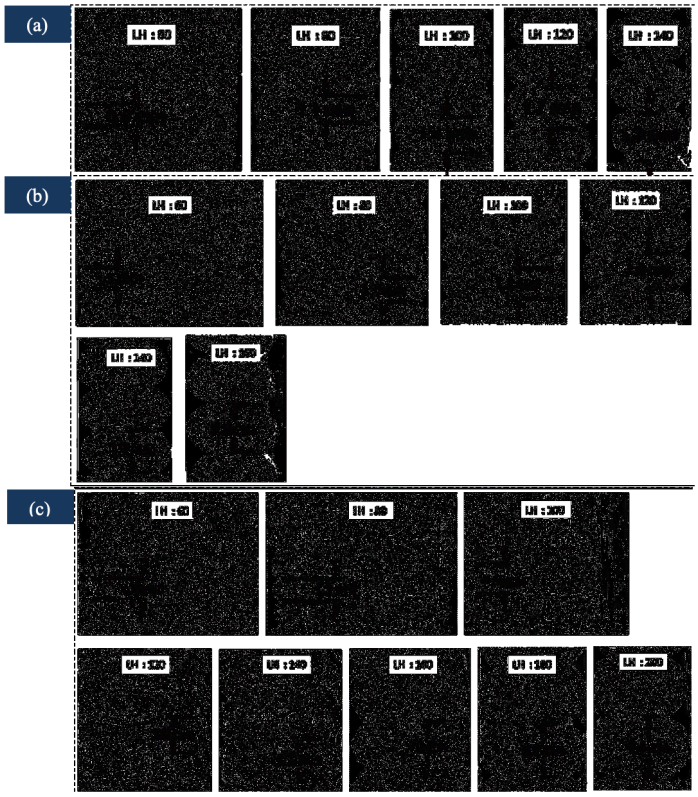

Fig. 11. Layer height characteristics of robot-assisted 3D-printed clay specimens under different nozzle diameters: (a) Nozzle diameter of 3.0 mm with layer heights ranging from LH60 to LH140; (b) Nozzle diameter of 4.0 mm with layer heights ranging from LH60 to LH160; and (c) Nozzle diameter of 5.0 mm with layer heights ranging from LH60 to LH200.

sively rougher, with more visible layer lines and increased surface irregularities [67]. These irregularities were particularly pronounced in specimens printed with the 5.0 mm nozzle diameter, where the thicker layers resulted in noticeable step lines between successive layers, detracting from the overall aesthetic and structural uniformity of the specimen.

Print speed also played a significant role in determining layer consistency. Lower print speed (150-250 mm/s) allowed the material to be deposited more slowly and uniformly, resulting in smoother, more consistent layers with fewer gaps or overlaps. These defects were especially common in specimens printed with the larger 5.0 mm nozzle diameter, where the combination of high print speed and thick layers led to excessive material flow and layer separation, contributing to the formation of voids within the structure. Such visual defects not only compromise the surface finish but also weaken the interlayer bonds, ultimately reducing the mechanical strength of the printed object [68,69]. Therefore, from a visual standpoint, the optimal balance between nozzle diameter and print speed is critical for achieving high-quality prints with consistent, defect-free layers. In addition to surface finish, the visual analysis revealed several key defects—such as voids,

cracks, and sagging—that directly impacted the structural integrity of the printed specimens. Voids, which are air pockets trapped within the material, were particularly prevalent in specimens printed with higher layer heights (LH160) and larger nozzle diameters (5.0 mm). These voids occurred due to incomplete material deposition and insufficient bonding between the thick layers, leading to weak points within the structure [70, 71]. In contrast, specimens printed with smaller layer heights (LH60) exhibited fewer voids, as the finer layers allowed for better compaction and interlayer adhesion, resulting in more structurally sound objects.

The defects identified through visual analysis—such as voids, cracks, and sagging—had a direct correlation with the mechanical performance of the printed specimens, particularly their compressive strength and flexural resistance. Specimens with smoother surfaces and more consistent layer deposition, typically those printed with smaller nozzles and lower print speed, exhibited higher mechanical strength. The lack of visible voids and cracks in these specimens suggested that the material had been evenly deposited and adequately compacted, leading to stronger interlayer bonds and greater resistance to compressive and flexural forces. In contrast, specimens with rougher surfaces, more pronounced layer lines, and visible voids—such as those printed with larger nozzles and higher print speed—showed significantly reduced mechanical strength. The presence of these visual defects weakened the interlayer cohesion, making the structure more susceptible to failure under mechanical stress. Additionally, the degree of sagging observed in the specimens was found to have a strong influence on their dimensional accuracy and overall structural stability. Specimens with minimal sagging, typically those printed with moderate moisture content and smaller layer heights, maintained their intended geometric shape and exhibited greater resistance to deformation. In contrast, specimens with excessive sagging, often those with higher water content or larger layer heights, experienced significant dimensional deviations and reduced mechanical performance. These findings highlight the importance of visual analysis as a diagnostic tool for identifying potential weaknesses in the printed structure before mechanical testing, allowing for a more comprehensive evaluation of the 3D-printing process.

The visual analysis of printed specimens provides valuable insights into how process parameters such as nozzle diameter, print speed, layer height, and material composition influence the surface quality and structural integrity of 3D-printed clay. By correlating visual defects with mechanical performance, this study highlights the critical importance of optimizing these parameters to minimize defects and enhance the overall quality of the printed structures. The findings from this analysis will guide future research in refining the robot-assisted clay 3D-printing process, with a particular focus on improving layer consistency, reducing voids and cracks, and maintaining dimensional accuracy across a wide range of applications.

3.4 Optimization of process parameters

The optimization of process parameters in robot-assisted clay 3D-printing plays a pivotal role in enhancing the overall quality, efficiency, and mechanical properties of printed structures. The interaction between key variables—such as nozzle diameter, print speed, layer height, and material composition—has a significant impact on the performance of the final prod-

uct. To achieve optimal results, a delicate balance must be maintained among these parameters to ensure high-quality outputs, structural integrity, and adaptability to various applications, particularly in construction and architecture. This study systematically explores how adjusting these process parameters affects the mechanical properties of printed clay, providing insights that are crucial for fine-tuning the 3D-printing process and expanding its applicability [72, 73].

The size of the nozzle used in 3D-printing is one of the most critical factors influencing the resolution and structural cohesion of printed objects. In this study, three nozzle diameters (3.0 mm, 4.0 mm, and 5.0 mm) were tested to evaluate their effect on compressive strength, flexural resistance, and water absorption. Smaller nozzle diameters were found to produce finer layers, leading to increased layer cohesion and higher mechanical strength. Specifically, the 3.0 mm nozzle produced printed objects with the highest compressive and flexural strengths, achieving maximum values of 8.5 MPa and 4.2 MPa as shown Fig. 12, respectively. This can be attributed to the reduced layer thickness and improved interlayer bonding, which collectively enhance the overall structural integrity. Conversely, larger nozzles (e.g., 5.0 mm) produced thicker layers, which resulted in weaker bonding between successive layers, leading to decreased mechanical performance. Interlayer defects negatively impacted the structural performance of the printed objects. The data show that the optimal layer height for achieving high mechanical performance in robot-assisted clay 3D-printing is in the lower range (LH60-LH100), especially when using smaller nozzles and slower print speed. These findings suggest that optimizing material composition is as critical as fine-tuning the mechanical parameters of the 3D-printing process. The combination of a moderate water-to-clay ratio, smaller nozzle diameters, lower print speed, and smaller layer heights emerged as the most effective configuration for maximizing the mechanical properties of the printed clay structures [6].

Print speed, the speed at which material is extruded, also significantly affects print quality. Lower print speed (150-250 mm/s) allowed for more precise material deposition, ensuring better bonding between layers and reducing the likelihood of void formation [74-76]. The study identifies an optimal print speed range of 150-250 mm/s for balancing print speed with structural quality, particularly when using smaller nozzles similar to 3.0 mm. Layer height, the vertical distance between successive printed layers, plays a crucial role in determining the overall surface finish and strength of the printed object. Smaller layer heights (LH60) resulted in smoother surface finishes and stronger interlayer bonds, which significantly improved the compressive and flexural strength of the printed specimens.

As shown in Fig. 12(a), optimizing the 3D-printing of clay in a robot-assisted process involves carefully balancing nozzle diameter, layer height, and print speed to achieve structural integrity, material efficiency, and print quality. The linear relationship between nozzle diameter (x (mm)) and layer height (y (mm)) is expressed by the equation $y = 0.5x$ with an $R^2 = 1.000$, indicating a perfect correlation. This suggests that increasing nozzle diameter allows for proportionally thicker layers, which can speed up printing but may reduce detail. For clay, this means that larger nozzle diameters can improve efficiency by allowing higher layer heights without compromising

the material's unique structural properties. However, this optimization requires finding a balance, as thicker layers can reduce surface resolution, while finer layers, although offering better detail, may weaken inter-layer adhesion [77, 78]. Additionally, controlling the print speed is crucial for consistent material flow, ensuring stable layer deposition without deformities, and achieving a cohesive print, especially important for materials like clay with specific flow and drying characteristics. In addition, Fig. 12(b) demonstrates a linear relationship between nozzle diameter (x) and print speed (V, (mm/s)), represented by the equation $V = 100x + 750$ with $R^2 = 1.000$, indicating that as nozzle diameter increases, the print speed decreases at a constant rate. This inverse relationship is crucial for controlling material flow and avoiding over-extrusion, which can cause print deformities, and under-extrusion, which weakens layer adhesion. For clay, this balance ensures consistent layer deposition, enhancing the structural integrity and dimensional accuracy of the printed object. Larger nozzle diameters allow higher layer heights but require a reduced print speed to prevent excess material deposition. Therefore, fine-tuning these parameters enables optimal printing speed without compromising surface detail or structural stability, which is essential for the unique properties of clay in 3D-printing applications [28, 79].

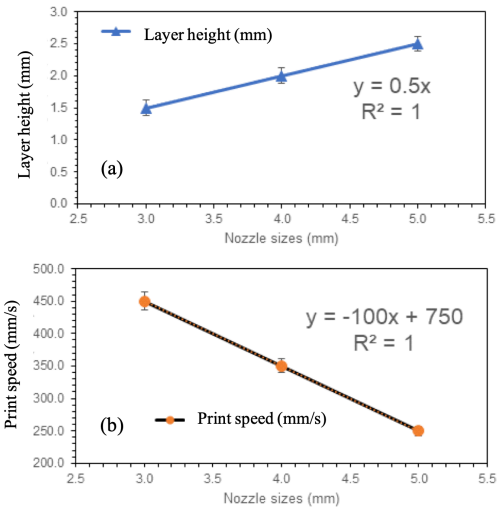

Fig. 12. Optimization of process parameters: (a) Layer height in mm and (b) Print speed (mm/s).

4. Discussion

The optimization of process parameters involved in robot-assisted clay 3D-printing poses a highly complex and multifaceted challenge that requires a meticulous, thorough examination of numerous variables, including but not limited to nozzle diameter, print speed, layer height, and the specific composition of the material used. These intricate parameters not only exert a significant influence on the mechanical properties exhibited by the printed objects, but they also play an essential and critical role in determining key factors such as surface quality, dimensional accuracy, and the overall structural integrity of the printed specimens, all of which are vital for the success of the additive manufacturing process [80]. The comprehensive findings derived from this study provide several important and profound insights into the intricate interactions among these various factors and how they collectively impact the performance and durability of 3D-printed clay structures, thereby establishing a robust foundation for future advancements and innovations in the field of clay-based additive manufacturing.

This study investigated the crucial and pivotal role that nozzle diameter plays in influencing both the mechanical strength and the visual quality of the printed objects produced through this advanced manufacturing process. Smaller nozzles, specifi-

cally those measuring 3.0 mm in diameter, which facilitate a finer deposition of layers, consistently yielded specimens that exhibited markedly higher compressive and flexural strengths, in addition to smoother surface finishes and a noticeable reduction in the presence of visible defects. This particular outcome can be fundamentally attributed to the enhanced interlayer bonding that is facilitated by the utilization of the smaller nozzle diameter, which ultimately results in the creation of denser, more cohesive, and structurally sound printed objects [81, 82]. Conversely, the employment of larger nozzles, specifically those measuring 4.0 mm and 5.0 mm in diameter, produced thicker layers characterized by inferior interlayer adhesion, which consequently led to a deterioration in mechanical performance and a more pronounced occurrence of surface irregularities. These critical findings illuminate the inherent tradeoff that exists between printing resolution and operational speed; while larger nozzles enable a more rapid deposition of material, they simultaneously compromise the quality and structural strength of the printed objects being produced [83]. Thus, it is imperative that the selection of nozzle diameter be meticulously calibrated and optimized in accordance with the specific requirements and objectives of the project at hand, thereby achieving a delicate balance between the necessity for precision and the constraints imposed by time and material efficiency.

Another pivotal and critical finding that emerged from this research study is the profound influence exerted by both print speed and layer height on the mechanical as well as visual properties of the printed structures created through the 3D-printing process. The study conclusively demonstrated that the implementation of slower print speed, specifically within the range of 150 to 250 mm/s, resulted in an enhanced layer cohesion and significantly smoother surface finishes, whereas the application of higher print speed, exceeding 350 mm/s, led to the manifestation of defects such as voids and poor interlayer adhesion, which ultimately weakened the overall structural integrity of the printed objects. Similarly, the utilization of smaller layer heights, specifically LH60, was associated with a marked improvement in compressive strength and flexural resistance, a phenomenon attributable to the finer stacking of layers and the consequent enhancement of material compaction achieved through this method. In stark contrast, the employment of larger layer heights, such as LH160, increased the propensity for void formation and resulted in a deterioration of mechanical properties. These compelling results underscore the critical importance of meticulously controlling both the print speed and layer height parameters to achieve optimal structural integrity in the context of 3D-printed clay objects [84, 85]. While it may be tempting to favor higher print speed and larger layer heights in order to expedite the printing process, such decisions introduce significant risks concerning structural stability and mechanical performance, thereby suggesting that these parameters should be carefully optimized with a focus on prioritizing quality over the mere acceleration of production speed.

4.1 Material composition and process parameters

In addition to considering critical factors such as nozzle diameter, print speed, and layer height, it is imperative to recognize that the composition of the clay mixture itself significantly contributes to the overall success and efficacy of the 3D-

printing process, underscoring the multifaceted nature of this technology [86-88]. The intricate interaction between material composition and process parameters becomes particularly evident when examining the formation of various visual defects, which can include voids, cracks, and sagging, all of which adversely affect the quality of the printed output. Voids, which were observed to be more prevalent in specimens that were printed using larger nozzle diameters in conjunction with higher layer heights, serve as indicators of inadequate material deposition as well as insufficient bonding between successive layers, which is critical for structural integrity. The presence of these defects was further exacerbated by the implementation of high print speed alongside large layer heights, thereby underscoring the necessity for meticulous coordination between the inherent properties of the material and the parameters governing the printing process [3]. In a similar manner, the occurrence of cracks within specimens characterized by lower moisture content strongly suggests that the optimization of the material's composition is vital in order to alleviate stress concentrations within the printed layers, particularly when employing smaller nozzle diameters and slower print speed during the printing process.

In robot-based clay and sintered clay 3D-printing, anisotropy arises from the layer-by-layer deposition process, weakening interlayer bonding and making mechanical properties (compressive, flexural, and tensile) more directional. These challenges can be mitigated through specific printing strategies, improved interlayer bonding control, and advanced characterization techniques, thereby enhancing structural robustness and surface quality. In addition, to understand microstructural evolution and degradation mechanisms over time, a more systematic assessment of long-term environmental durability-especially under varying humidity, temperature fluctuations, and cyclic exposure-needs to be conducted. Therefore, future studies should focus on linking anisotropic interfaces to moisture-transport characteristics and on developing predictive models to simulate long-term performance, including, but not limited to, practical issues of cost, complexity, and large-scale deployment.

4.2 Implications for large-scale applications

The ramifications stemming from this comprehensive research endeavor extend far beyond the confines of the laboratory environment, revealing an expansive and noteworthy potential for large-scale applications specifically within the realms of the construction and architectural sectors [89,90]. The innovative capability to fabricate clay structures that are not only robust and durable but also visually striking, utilizing the advanced technology of robot-assisted 3D-printing, unveils a plethora of exhilarating opportunities for creating sustainable and customizable building solutions that could redefine industry standards. The findings derived from this study indicate that through the meticulous optimization of critical process parameters—including but not limited to nozzle diameter, print speed, layer height, and the composition of materials—architects and engineers are empowered to generate high-quality clay structures that not only adhere to specific design criteria but also significantly diminish waste and mitigate the ecological footprint typically associated with conventional construction methods [51, 91-93].

Nevertheless, it is crucial to ac-

knowledge that a multitude of challenges persists in the endeavor to translate these significant findings into viable and practical applications within real-world settings. Among the most formidable obstacles hindering the widespread acceptance of clay-based 3D-printing technology is the inherent issue of scalability associated with the process. Although employing smaller nozzle diameters in conjunction with reduced print speed can yield prints of superior quality, this approach inadvertently extends the duration necessary to complete large-scale construction projects, thereby posing potential limitations to the feasibility of implementing this innovative technology for the construction of substantial edifices [93]. Consequently, it is imperative that future research initiatives prioritize the development of sophisticated algorithms and automated systems designed to effectively optimize the delicate equilibrium between print speed and quality, potentially leveraging machine learning or artificial intelligence techniques to dynamically adjust process parameters in real time, utilizing feedback derived from an array of sensors or imaging devices. Moreover, an additional avenue warranting exploration for future research endeavors lies in the formulation of novel material compositions that may significantly enhance both the mechanical properties and workability of clay specifically tailored for 3D-printing applications [94]. The strategic incorporation of various additives, such as fibrous materials or recycled components, has the potential to not only bolster the strength and durability of the printed constructs but also contribute positively to their sustainability profile.

One of the benchmarks for comparison and for explicitly addressing anisotropy, further to situate the study within scalable, eco-friendly architectural contexts. In particular, the mechanical properties and structural performance of robot-assisted 3D-printed clay and sintered clay are now compared with those of traditional construction materials to illuminate their structural feasibility, eco-friendly architectural applications, and sustainability advantages, including reduced embodied carbon [78,95,96] and greater local material availability. Process efficiency, including material utilization, construction speed, and waste reduction, is also emphasized during scaling-up. Optimizing printing parameters, layer orientation, and deposition intervals is introduced to alleviate directional weaknesses and improve performance reliability [97].

5. Conclusion

Based on the developed robot-assisted extrusion system and extensive parametric data, the effect of printing parameters on 3D-printed clay and sintered clay material mechanical performance, structural integrity, as well as surface quality is investigated. The main conclusions are drawn as follows: (1) The study demonstrated that nozzle diameter plays a pivotal role in the overall strength and durability of printed clay structures. Smaller nozzle diameters (3.0 mm) produced more compact and cohesive layers, leading to higher compressive and flexural strengths. The finer deposition of material facilitated stronger interlayer bonding, which directly contributed to the improved mechanical properties observed in the specimens. Conversely, larger nozzle diameters (5.0 mm) resulted in weaker interlayer cohesion and more pronounced surface defects, such as visible layer lines and rough finishes. These findings suggest that smaller nozzle diameters are more

appropriate for applications requiring high structural integrity, while larger nozzles may be suitable for less critical designs where faster print speeds are prioritized. (2) The results indicate that slower print speed (150-250 mm/s) and smaller layer heights (LH60) consistently yielded the best outcomes in terms of surface quality and mechanical performance. Lower print speed allowed for more controlled material deposition, reducing the risk of voids and defects, while smaller layer heights resulted in finer layer stacking and better material compaction. These optimized settings are crucial for ensuring uniform layer deposition, which enhances the printed structure's resistance to both compressive and flexural forces. Higher print speed and larger layer heights were associated with defects such as voids, cracks, and poor interlayer bonding, which weakened the overall structure. Therefore, precise control over these parameters is essential for achieving high-quality, durable clay prints. (3) The findings from this study have practical implications for the use of robot-assisted 3D-printing in construction, particularly in creating sustainable and customizable building components. The ability to optimize process parameters based on the specific requirements of each project allows for greater flexibility in design and material use. By fine-tuning nozzle diameter, print speed, layer height, and material composition, engineers and architects can produce high-quality, structurally sound clay-based components that meet the demands of modern construction while minimizing environmental impact.

One of the most promising applications of this technology is in the development of sustainable construction methods that reduce material waste and energy consumption. Clay, as a natural and abundant material, offers significant potential for eco-friendly construction, particularly when combined with the precision and efficiency of robotic 3D-printing. This study shows that by optimizing process parameters, it is possible to create strong, durable clay structures with minimal material waste, making this technology an attractive option for future construction projects focused on sustainability.

Acknowledgements

This research was supported by Thailand Science Research and Innovation (TSRI) for the fiscal year 2024. The authors gratefully acknowledge Faculty of Industrial Technology, Phranakhon Rajabhat University, Bangkok, Thailand for providing access to research facilities and equipment.

References

[1] Douglas R, Faria P, Lucas SS. Additive manufacturing of earth-based materials: a literature review on mortar composition, extrusion, and processing earth materials. Materials. 2023;17(1):202.

[2] Abdukarimov TTo. Material-in-the-loop fabrication: a vision-based adaptive clay 3D-printing workflow on indeterminate sand surfaces. Commun Comput Inf Sci. 2023;1828:385-400.

[3] Kontovourkis O, Tryfonos G. Integrating parametric design with robotic additive manufacturing for 3D clay printing: an experimental study. In: Proceedings of the 35th International Symposium on Automation and Robotics in Construction (ISARC); 2018 Jul 22-25; Berlin, Germany. p. 948-955.

[4] Yuan PF, Meng H, Yu L, Zhang L. Robotic multi-dimensional printing based on structural performance. In: Yuan PF, Yi H, editors. Digital soft-architecture. Cham: Springer; 2016. p. 77-88.

[5] Ndarowa TE, Mahachi J, Ikotun BD. A review of optimization of limestone and calcined clay cement (LC3) concrete mixtures for 3D printing. In: Proceedings of the 9th International Conference on Civil, Structural and Transportation Engineering (ICCSTE '24); 2024 May 19-21; Niagara Falls, Canada. Ottawa (ON): Avestia Publishing; 2024. Article No. 191.

[6] Rückrich S, Agranati G, Grobman YJ. Evaluating clay characteristics for printable geo-materials: a case study of clay-sand mixes. Buildings. 2024;14(6):1576.

[7] Li H, Wei JJ, Khayat KH. 3D printing of fiber-reinforced calcined clay-limestone-based cementitious materials: from mixture design to printability evaluation. Buildings. 2024;14(6):1666.

[8] Koga Y, Kerrick H, Chitta S. On CAD informed adaptive robotic assembly. In: 2022 IEEE/RSJ International Conference on Intelligent Robots and Systems (IROS); 2022 Oct 23-27; Kyoto, Japan. IEEE; 2022. p. 11984-91.

[9] Lacny C, Zhang J. Computer vision-based geometry mapping and matching of building elements for construction robotic applications. In: Computing in civil engineering 2021. Reston (VA): American Society of Civil Engineers; 2022. p. 556-64.

[10] Nicholas P, Rossi G, Williams E, Bennett M, Schork T. Integrating real-time multi-resolution scanning and machine learning for conformal robotic 3D printing in architecture. Int J Archit Comput. 2020;18(3):286-306.

[11] Zhang Y, Zhang K, Chen K, Xu Z. Real time scanning-modeling system for architecture design and construction. Appl Innov Technol Ind. 2020;2(1):15-24.

[12] Tish D, King N, Cote N. Highly accessible platform technologies for vision-guided, closed-loop robotic assembly of unitized enclosure systems. Constr Robot. 2020;4(1-2):3-17.

[13] Izmaylov DV, Tolstoba ND, Bodrov K. Computer vision system selection for control of rapid prototyping processes. In: Proceedings of the SPIE 10684, Optical Sensing and Detection V; 2018 May 24; Brussels, Belgium. SPIE; 2018. Article No. 106840N.

[14] Pigram D, Maxwell I, McGee W. Towards real-time adaptive fabrication-aware form finding in architecture. In: Yuan PF, Yi H, editors. Digital soft-architecture. Cham: Springer; 2016. p. 433-47.

[15] Zhu W, Wang P, Li F, Su J, Qiao H. Real-time 3D model-based tracking of workpiece with monocular camera. In: Proceedings of the 2015 IEEE/SICE International Symposium on System Integration (SII); 2015 Dec 11-13; Nagoya, Japan. IEEE; 2015. p. 730-5.

[16] Song Y, Vergeest JSM, Wiegers T. Interactive freeform clay modeling supported by 3D scanning and robot machining. In: Proceedings of the ASME 2004 Design Engineering Technical Conferences and Computers and Information in Engineering Conference (DETC2004); 2004 Sep 28-Oct 2; Salt Lake City (UT). New York (NY): ASME; 2004. p. 1113-21.

[17] Sithiwichankit C. Machine vision integrated three-dimensional printing system [dissertation]. Bangkok: Chulalongkorn University; 2019.

[18] Chen L, Chen Q, Tan X, Liu S, Xue X. Development of an extrusion-based five-axis 3D printing system for manufacturing of complex parts. In: Proceedings of the 2023 IEEE International Conference on Advanced Robotics and Mechatronics (ICARM); 2023 Jul 8-10; Sanya, China. IEEE; 2023. p. 411-6.

[19] Ruscitti A, Tapia C, Rendtorff NM. A review on additive manufacturing of ceramic materials based on extrusion processes of clay pastes. Cerâmica. 2020;66(380):354-69.

[20] Li W, Leu MC. Material extrusion based ceramic additive manufacturing. In: Additive manufacturing of metals: the technology, materials design and applications. ASM International; 2020.

[21] Ko M, Shin D, Ahn H, Park H InFormed ceramics: multi-axis clay 3D printing on freeform molds In: Willmann J, Block P, Hutter M, Byrne K, Schork T, editors Robotic fabrication in architecture, art and design 2018 Cham: Springer; 2018 p 297-308.

[22] Chen Z, Li Z, Li J, Liu C, Lao C, Fu Y, et al 3D printing of ceramics: a review J Eur Ceram Soc 2019;39(4):661-87.

[23] Zhang L High-precision multi-axis 3D printer Patent CN106985474A 2017 Aug 1.

[24] Park JJ, Kim SI 3d multi-axis three-dimensional printer having exchangeable extruder-integrated printer head Patent KR101633513B1 2016 Jun 24.

[25] Gang X, Zhen S, Xue L, Feiyue W Multi-nozzle 3D printer and method for controlling speed and precision of multi-nozzle 3D printer Patent US9199411B2 2014.

[26] Wu Y, Lan J, Wu M, Zhou W, Zhou S, Ye H, et al Rheology and printability of a porcelain clay paste for DIW 3D printing of ceramics with complex geometric structures ACS Omega 2024;9(23):25275-86.

[27] Song K, Yang S, Shao N, Zhao Y, Zhao Y, He P, et al Highly strengthening and toughening biomimetic ceramic structures fabricated via a novel coaxially printing J Adv Ceram 2024;13(9):1387-400.

[28] Asaf O, Bentur A, Larianovsky P, Sprecher A From soil to printed structures: a systematic approach to designing clay-based materials for 3D printing in construction and architecture Constr Build Mater 2023;399:133783.

[29] Zhang H, Zhao K, Liu D, Hu Q, Lammer H Development of fused deposition modeling using five-axis machine and printing methods Res Sq [Preprint] 2021.

[30] Jauk J, Vasatko H, Gosch L, Ristoski K, Füssl J, Stavric M Coextrusion of clay-based composites: using a multi-material approach to achieve gradient porosity in 3D-printed ceramics Ceramics 2023;6(4):2194-213.

[31] Lahaie RG, Hansen CJ, Kazmer D Development of fused deposition modeling of multiple materials (FD3M) through dynamic coaxial extrusion 3D Print Addit Manuf 2023;10(6):1224-37.

[32] Victor EY, Leng Y, Donghun P 5-axis three-dimensional manufacturing Patent US10434714B2 2019.

[33] Shen H, Diao H, Yue S, Fu J Fused deposition modeling five-axis additive manufacturing: machine design, fundamental printing methods and critical process characteristics Rapid Prototyp J 2018;24(8):1245-56.

[34] Maidin S, Mohamed ASR, Akmal S, Mohamed SB, Wong JHU Feasibility study of technology integrated vacuum fused deposition modeling to reduce staircase effect J Fundam Appl Sci 2018;10(1S):617-28.

[35] Nazarian S, Duarte JP, Bilén SG, Memari AM, Radlińska A, Meisel NA, et al Additive manufacturing of architectural structures: an interplay between materials, systems, and design In: Labonnote N, Høyland K, editors Additive manufacturing in construction Cham: Springer; 2021 p 289-314.

[36] Liu S Structural design of a novel rotary platform 3D printer J Phys Conf Ser 2024;2798(1):012023.

[37] Hassan H, Rodriguez-Ubinas E, Al Tamimi A, Trepci E, Mansouri A, Saqer K, et al Towards innovative and sustainable buildings: a comprehensive review of 3D printing in construction Autom Constr 2024;164:105417.

[38] Jambhulkar S, Ravichandran D, Sundaravadivelan B, Song K A hybrid 3D printing for highly-efficient nanoparticle micropatterning J Mater Chem C 2023;11(13):4398-409.

[39] Villa A, Gianchandani P, Baino F Sustainable approaches for the additive manufacturing of ceramic materials Ceramics 2024;7(1):331-62.

[40] Li X, Baldacchini T, Chen Y An investigation of integrated multi-scale 3D printing for hierarchical structures fabrication J Micro Nano-Manuf 2022;10(1):011003.

[41] ASTM International ASTM C324-01(2007): Standard test method for free moisture in ceramic whiteware clays West Conshohocken (PA): ASTM International; 2007.

[42] Dostrašil P Implementation of specific displacement diagrams for the control of kinetic sculptures with Yaskawa electronic cams In: Beran T, editor Mechatronics 2017 Cham: Springer; 2017 p 431-8.

[43] Cruz IMG, Bertoncelli K, Souza TDA, Sotana R, Aguiar A, Pereira V Symbolic and numerical mathematical modeling of the Jacobian of the Yaskawa Motoman - Gp7 robot using Matlab J Robot Autom Res 2022;3(2):167-76.

[44] Jin Y, Gruver WA Experimental results for hybrid stable neurocontrol of a Yaskawa industrial robot In: Proceedings of the 1996 IEEE International Conference on Robotics and Automation; 1996 Apr 22-28; Minneapolis, MN IEEE; 1996 p 3137-42.

[45] Baklouti S, Gallot G, Viaud J, Subrin K On the improvement of ROS-based control for teleoperated Yaskawa robots Appl Sci 2021;11(16):7190.

[46] Santos G, Varaschim FH, Almeida JPLSD Estudo da cinemática do robô manipulador Yaskawa Motoman 6R baseado em testes de laboratório In: Anais do 3° Congresso Internacional de Engenharia Mecânica e Industrial 2022.

[47] Cong L, Jialin L, Jiemei G, Honghao G, Yuming H. Formula of ceramic 3D printing mud. Patent CN108689694A. 2018 Oct 23.

[48] ASTM International. ASTM C1161-18: Standard test method for flexural strength of advanced ceramics at ambient temperature. West Conshohocken (PA): ASTM International; 2018.

[49] ASTM International. ASTM C1424-15(2019): Standard test method for monotonic compressive strength of advanced ceramics at ambient temperature. West Conshohocken (PA): ASTM International; 2019.

[50] ASTM International. ASTM C373-18: Standard test method for water absorption, bulk density, apparent porosity, and apparent specific gravity of fired whiteware products. West Conshohocken (PA): ASTM International; 2023.

[51] Yu YJ, Zhang G, Xiao Q, Ji A, Feng Y, Zhu GR, et al. 3D printer nozzle structure form optimal structural analysis. Processes. 2024;12(7):1482.

[52] Balani SB, Mokhtarian H, Salmi T, Coatanéa E. An investigation of the influence of viscosity and printing parameters on the extrudate geometry in the material extrusion process. Polymers. 2023;15(9):2202.

[53] Montañez YT. Toward an improved understanding for design of material extrusion additive manufacturing process-based 3D printers-a computational study. Adv Theory Simul. 2022;5(11):2200704.

[54] Elkaseer A, Chen KJ, Kuchta M, Scholz S. On the quantitative assessment of the effect of multiple process parameters on the printed layer height in 3D inkjet printing. Virtual Phys Prototyp. 2023;18(1):e2269898.

[55] Nair SAO, Tripathi A, Neithalath N. Examining layer height effects on the flexural and fracture response of plain and fiber-reinforced 3D-printed beams. Cem Concr Compos. 2021;124:104254.

[56] Bintara RD, Lubis DZ, Pradana YRA. The effect of layer height on the surface roughness in 3D printed polylactic acid (PLA) using FDM 3D printing. IOP Conf Ser Mater Sci Eng. 2021;1034(1):012096.

[57] Patel SY, Desai CK. Effect of layer height on tensile strength of fused deposited modeling printed carbon polylactic acid part. Indian Sci J Res Eng Manag. 2024;8(5):1-6.

[58] Chen MY, Pang R, Lai MK. Investigation on layer thickness on mechanical properties and dimension accuracy in fused deposition modelling 3D printing. Mater Sci Forum. 2024;1113:9-14.

[59] Fan JZ. Research of stepover for 3D surface machining. Coal Mine Mach. 2008;29(5):71-3.

[60] Karimi N, Bozorgnia Tabary SAA, Fayazfar H. In-depth investigation and industry plan for enhancing surface finishing of 3D printed polymer composite components: a critical review. J Appl Polym Sci. 2024;141(31):e55494.

[61] Yadav A, Poorna B, Dileep D, Prakash P, Sai K, Sureddi AR, et al. An experimental examination on surface finish of FDM 3D printed parts. Mater Today Proc. 2023.

[62] Bayrak AT, Shaban N, Choubi SS, Tuncer E, Yang SH, Yilmaz HD, et al. Spatial variation of physical, mechanical, and thermophysical properties of 3D printed concrete across a full-scale wall. Constr Build Mater. 2024;433:136574.

[63] Borella PS, Alvares LAS, Ribeiro MTH, Moura GF, Soares CJ, Zancopé K, et al. Physical and mechanical properties of four 3D-printed resins at two different thick layers: an in vitro comparative study. Dent Mater. 2023;39(9):835-44.

[64] Yang L, Sepasgozar SME, Shirowzhan S, Kashani A, Edwards DJ. Nozzle criteria for enhancing extrudability, buildability and interlayer bonding in 3D printing concrete. Autom Constr. 2023;146:104671.

[65] Djokikj J, Avramov N, Nestorovski B, Hristova EH. Compressive strength of 3D fabricated parts: experimental and numerical studies. TEM J. 2024;13(1):217-25.

[66] Manikandan K, Jiang X, Singh AA, Li B, Qin H. Effects of nozzle geometries on 3D printing of clay constructs: quantifying contour deviation and mechanical properties. Procedia Manuf. 2020;48:848-54.

[67] Chen KJ, Elkaseer A, Scholz S, Hagenmeyer V. On the correlation between preprocessing workflow and dimensional accuracy of 3D printed parts in high-precision material jetting. Addit Manuf. 2024;89:104335.

[68] Ayatollahi MR, Nabavi-Kivi A, Salamatian Hosseini S, Khosravani MR. Effect of nozzle diameter and raster orientation on tensile and fracture behavior of FDM-PLA specimens under mixed-mode I/II loading. Fatig Fract Eng M. 2024;47(9):3158-72.

[69] Abdulridha H, Abbas TF, Bedan AS. Investigate the effect of chemical post processing on the surface roughness of fused deposition modeling printed parts. Adv Sci Technol Res J. 2024;18(3):284-94.

[70] Bianchi I, Mancia T, Mignanelli C, Simoncini M. Effect of nozzle wear on mechanical properties of 3D printed carbon fiber-reinforced polymer parts by material extrusion. Int J Adv Manuf Technol. 2024;131:3681-91.

[71] Nigam A, Tai BL. Effects of in-process surface finishing on part strength in polymer material extrusion additive manufacturing. Addit Manuf. 2024;80:103960.

[72] Pemas S, Sougioultzi K, Stefanidou M, Kouroutzidou A, Konstantinidis K, Pechlivani E. Enhancing clay-based 3D-printed mortars with polymeric mesh reinforcement techniques. Polymers. 2024;16(15):2182.

[73] Chen F. Optimizing 3D printing materials and parameters for robotics applications. In: Proceedings of the 9th International Conference on Civil, Structural and Transportation Engineering (ICCSTE'24); 2024 May 19-21; Niagara Falls, Canada. Avestia Publishing; 2024.

[74] Awasthi P, Kumar A, Pandey PM, Banerjee SS. Optimization of process parameters of 3D printed thermoplastic elastomeric materials using statistical modeling with particular reference to mechanical properties and print quality. Funct Compos Mater. 2024;5:11.

[75] Liu X, Hu J. Printability and interlayer bonding property of 3D printed fiber reinforced geopolymer (3DP-FRG). J Build Eng. 2024;90:109060.

[76] Xie J, Zhou X, Liu Y, Zhang JG, Wang S. Process parameters optimization for 3d printing of continuous carbon fiber reinforced composite. Materia (Rio J). 2024;29(2):e20240201.

[77] Fadaie S, Mehravar M, Webb DJ. Interfacial characterization of soil-3D printing materials. E3S Web Conf. 2024;544:01034.

[78] Alsa'di S, Zgoul M, AlAlaween WH, Al-Qawabah SM. Examining and modelling the effects of 3D fused deposition parameters. ES Mater Manuf. 2024;25:1197.

[79] Marković MP, Cingesar IK, Vrsaljko D. Maximizing mechanical performance of 3D printed parts through process parameter optimization. 3D Print Addit Manuf. 2023;10(6):1124-35.

[80] Ding CK, Wang J, Ma Y, Tu Y, Ma Y. Multi-objective Bayesian modeling and optimization of 3D printing process via experimental data-driven method. Qual Reliab Eng Int. 2024;40(6):3014-30.

[81] Zonoobi MA, Gorgani HH, Javahernehshan D. Experimental investigation and multi-objective optimization of FDM process parameters for mechanical strength, dimensional accuracy, and cost using a hybrid algorithm. Scientia Iranica. 2023;30(6):2105-20.

[82] Golan O, Lachman N. Process design and parameters interaction in material extrusion 3D printing: a review. Polymers. 2023;15(10):2280.

[83] Abas M, Habib T, Noor S, Salah B, Zimon D. Parametric investigation and optimization to study the effect of process parameters on the dimensional deviation of fused deposition modeling of 3D printed parts. Polymers. 2022;14(17):3667.

[84] Chohan JS, Kumar RS, Yadav A, Chauhan P, Singh S, Sharma S, et al. Optimization of FDM printing process parameters on surface finish, thickness, and outer dimension with ABS polymer specimens using Taguchi orthogonal array and genetic algorithms. Math Probl Eng. 2022;2022:2698845.

[85] Mozaffar M, Cao J. Additive manufacturing process design with differentiable simulations. arXiv. 2021.

[86] Shirmohammadi M, Goushchi SJ, Keshtiban PM. Optimization of 3D printing process parameters to minimize surface roughness with hybrid artificial neural network model and particle swarm algorithm. Complex Intell Syst. 2021;7:3101-14.

[87] Dey A, Yodo N. A systematic survey of FDM process parameter optimization and their influence on part characteristics. J Manuf Mater Process. 2019;3(3):64.

[88] Rebaioli L, Magnoni P, Fassi I, Pedrocchi N, Tosatti LM. Process parameters tuning and online re-slicing for robotized additive manufacturing of big plastic objects. Rob Comput Integr Manuf. 2019;55:181-93.

[89] Alabd MU, Temiz A. Optimization of annealing and 3d printing process parameters of pla parts. Int J 3D Print Technol Digit Ind. 2024;8(1):151-62.

[90] Petruse RE, Simion C, Bondrea I. Geometrical and dimensional deviations of fused deposition modelling (FDM) additive-manufactured parts. Metrology. 2024;4(3):363-79.

[91] Gajjar T, Yang C, Ye L, Zhang YX. Effects of key process parameters on tensile properties and interlayer bonding behavior of 3D printed PLA using fused filament fabrication. Prog Addit Manuf. 2024.

[92] Abas M, Khan I, Jan Z. An integrated approach of particle swarm optimization and grey relational analysis in multi-response optimization of fused deposition modeling. In: Management of systems, software engineering, and high-performance computing. IGI Global; 2024. p. 18-44.

[93] Sabev S, Chukalov K, Bakardzhiev V, Izmirliyan A. Optimizing 3d printing parameters to improve hardness and surface roughness. Environ Technol Resour. 2024;3:100-4.

[94] Raju S. Evaluating impact of different parameters in additive manufacturing for complex situations. Indian Sci J Res Eng Manag. 2024;8(5):1-7.

[95] Vaghefi E, Hosseini S, Afsharinejad AH, Prorok BC, Mirkoohi E. Additive manufacturing process parameter design for variable component geometries using reinforcement learning. Addit Manuf. 2024;86:104121.

[96] Shao C. Parameter optimization of 3D printing process for ceramic sculptures. Appl Math Nonlinear Sci. 2024;9(1).

[97] Schuller T, Jalaal M, Fanzio P, Galindo-Rosales FJ. Optimal shape design of printing nozzles for extrusion-based additive manufacturing. Addit Manuf. 2024;84:104130.